Journal of Organometallic Chemistry, 478 (1994) 95–102

Electronic structure and bonding in triple-decker complexes of Mn and Co with borole ligand(s). Photoelectron spectra and molecular orbital calculations

Rolf Gleiter [a], Isabella Hyla-Kryspin [a] and Gerhard E. Herberich [b]

[a] *Organisch-Chemisches Institut der Universität Heidelberg, Im Neuenheimer Feld 270, D-69120 Heidelberg (Germany)*
[b] *Anorganisch-Chemisches Institut der Technischen Hochschule Aachen, Professor-Pirlet-Straße 1, D-52074 Aachen (Germany)*

(Received October 15, 1993)

Abstract

The electronic structures of μ-($C_4H_4BCH_3$) $[Mn(CO)_3]_2$ (**5**) and ($C_4H_4BCH_3$)Co-μ-($C_4H_4BCH_3$)Mn$(CO)_3$ (**6**) have been derived by correlating the frontier MOs of the metal dimers $[Mn(CO)_3]_2^{2+}$ and $[Co(C_4H_4BCH_3)\ Mn(CO)_3]^{2+}$ with those of the central borole dianion $C_4H_4BCH_3^{2-}$. It is found that the interaction between the metal dimer and central borole ligand in **5** is stronger than in **6**. This finding is supported by the He (I) PE spectra of **5** and **6**. The interpretation of the spectra is based on INDO calculations, in which relaxation and correlation effects are taken into account by means of the Green's function method.

Key words: Cobalt; Manganese; Boron; Photoelectron spectroscopy; Molecular orbital calculations; Triple-decker complexes

1. Introduction

To understand metal–metal interactions in systems without any direct metal–metal bond we have started to investigate systems such as **1–4** [1–4]. In these studies we used molecular orbital (MO) calculations in association with data from photoelectron (PE) spectroscopy [1,6], cyclovoltammetry [2], and X-ray investigations [3,4].

In this paper we report on our studies on the triple-decker complexes **5** and **6**, which were prepared recently [5]. The results are compared with those for the triple decker **4** [6].

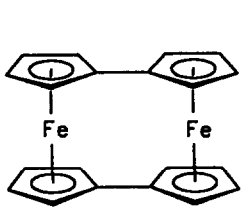

1

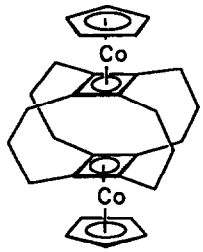

2

Correspondence to: Professor R. Gleiter.

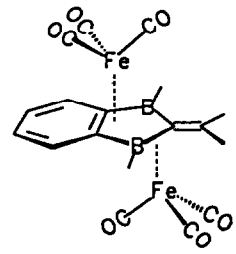

3

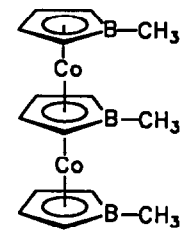

4

2. Results and discussion

2.1. Computational details

To gain an insight into the ground state electronic structure of **5** and **6** we adopted Hoffmann's fragment MO approach [7] based upon extended Hückel calculations [8] with standard parameters for all atoms [9]. The semiempirical INDO calculations were carried out by an improved INDO procedure [10] that was developed to simulate high-quality *ab initio* calculations on organometallic compounds. The non-validity of Koopmans' theorem in respect of ionizations from orbitals with strong metal character is well documented [11–13]. In the case of molecules with low symmetry the stan-

SSDI 0022-328X(93)21281-9

Elsevier Science S.A.

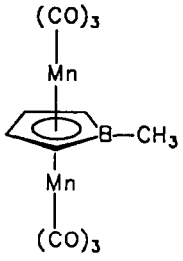

5

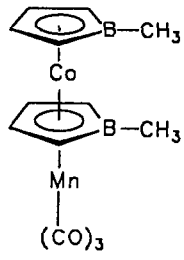

6

dard Δ SCF and Δ CI methods are not appropriate because of the variational collapse that usually occurs for the states that are not lowest in their representation.

In the present study we have chosen a many-body perturbational approach based on the Green's function method [14]. In this approach the relaxation and correlation effects in the ground and cationic states are explicitly taken into account. By analogy with previous studies [15] we adopted the following approximation for the self-energy part $\Sigma(\omega)$ in the inverse Dyson equation [16]:

$$\Sigma(\omega) = \Sigma^{(2)}(\omega) + \mathrm{D4} \qquad (1)$$

This expression contains second-order terms $\Sigma^{(2)}(\omega)$ to approximate the self-energy part and one third-order term, D4 [14]. The j^{th} vertical ionization potential $I_{v,j}^{\mathrm{GF2}}$, is related to the j^{th} canonical MO energy, ϵ_j, according to (2), if the inverse Dyson equation is solved via the diagonal variant:

$$-I_{v,j}^{\mathrm{GF2}} = \epsilon_j + \Sigma_{jj}^{(2)} + (\mathrm{D4})_{jj} \qquad (2)$$

This method was successfully applied to various metal complexes, either on the INDO [12,17] or *ab initio* level [18]. The geometry used for the calculations on the triple-decker complex of **5** was adapted from the reported X-ray structure for the closely related compound μ-$(C_4H_3R^1BR^2)[Mn(CO)_3]_2$ ($R^1 = C_2H_5$, $R^2 = C_6H_5$) [5]. The X-ray structure for the CoMn triple-decker complex **6** is not available. The geometrical parameters used for the calculations were deduced from the structures of complexes **5** [5] and **4** [4]. An eclipsed conformation of the borole ligands was assumed in order to take advantage of the C_s-symmetry. The borole rings were assumed to be planar.

2.2. *Electronic structure and bonding of the neutral molecules*

A convenient way of analyzing the bonding in the triple-decker complexes **5** and **6** is to build up the molecules from the metal dimer fragment and the central borole dianion. The borole dianion has six donating π-electrons and each metal atom can be considered as a d^6 species. A simplified interaction diagram in the case of **5** is shown in Fig. 1. The frontier orbitals of the $[Mn(CO_3)]_2^{2+}$ dimer can be easily derived as in-phase and out-of-phase combinations of the well known fragment MOs of two $Mn(CO)_3$ units [7]. They are shown on the left side of Fig. 1. The in-phase and out-of-phase combinations are not greatly split in energy because of the large distance between the metal atoms. For the sake of clarity we have omitted from Fig. 1 the empty levels 5a', 6a' and 3a", which are the bonding counterparts of the 7a', 8a' and 4a" levels and are left nonbonding with respect to the central ligand. On the right side of Fig. 1 we show the three donor π-orbitals of the borole dianion, 1a'(π_1), 2a"(π_2) and 3a'(π_3), together with two high lying, occupied σ-MOs, 2a' and 1a", mainly directed along the C–C and B–C σ bonds ("ribbon orbitals"). The two σ-levels can provide weak four-electron interactions with appropriate metal orbitals. The three π-orbitals match very well with the 8a', 4a" and 7a' MOs of the $[(CO)_3Mn \cdot Mn(CO)_3]^{2+}$ dimer. This gives rise to the occupied 1a', 1a" and the HOMO (7a') as well as the antibonding LUMO (5a"), 8a' and an empty high lying level of **5**. The "t_{2g}" like Mn-orbitals are clustered just below the HOMO and are followed by the two MOs 2a" and 2a' with dominant ligand σ-character (Fig. 1). Six electrons are stabilized in the 1a', 1a" and 7a' MOs of **5**. Together with 12 electrons from the "t_{2g}" like Mn levels and 12 electrons involved in Mn-carbonyl σ-bonds this yields a total of 30 VE, which corresponds to a stable situation [19].

The electronic structure of **6** can be analyzed similarly. A simplified interaction diagram is shown in Fig. 2. The frontier orbitals of the $CoMn^{2+}$ dimer are not described as in-phase or out-of-phase combinations of the valence MOs of the two metal fragments. They are split, and localized either on the $Mn(CO)_3$ or on the $Co(C_4H_4BCH_3)$ moiety (see left side of Fig. 2). Four additional levels appear in the valence region of the $CoMn^{2+}$ dimer, two MOs (7a', 4a") with dominant σ-character, and two MOs (4a', 2a")with dominant π_3 and π_2-character, of the terminal borole ligand. In this case there is also a good match between occupied and empty levels of the two fragments. The orbitals 8a' and 9a' of $CoMn^{2+}$ dimer interact with 3a' (π_3) of the borole dianion, while 5a" and 6a" interact with 2a" (π_2). This gives rise to the bonding levels 3a" and the HOMO (10a') the nonbonding LUMO (7a"), 11a' and the antibonding 8a", 12a' MOs of **6**. The "t_{2g}" like metal orbitals are now split by about 1.2 eV. The

"t_{2g}"-Mn levels are clustered below the HOMO, together with four σ-orbitals of the two borole ligands. The "t_{2g}" Co orbitals are located at lower energy (13.4–14 eV), together with two MOs, *viz.* 2a'' and 4a', with dominant π_2 and π_3 character, of the terminal borole ligand. The HOMO (10a') and 3a'' of **6** are predicted to be at higher energy than the HOMO (7a') and 1a'' MOs of **5** by 0.5 and 0.84 eV respectively, suggesting greater stabilizing interaction in **5** than in **6**.

2.3. *Photoelectron spectra and assignment*

The He(I) photoelectron spectra of **5** and **6** are presented in Fig. 3. Table 1 provides information on the computed ionization energies and assignments in

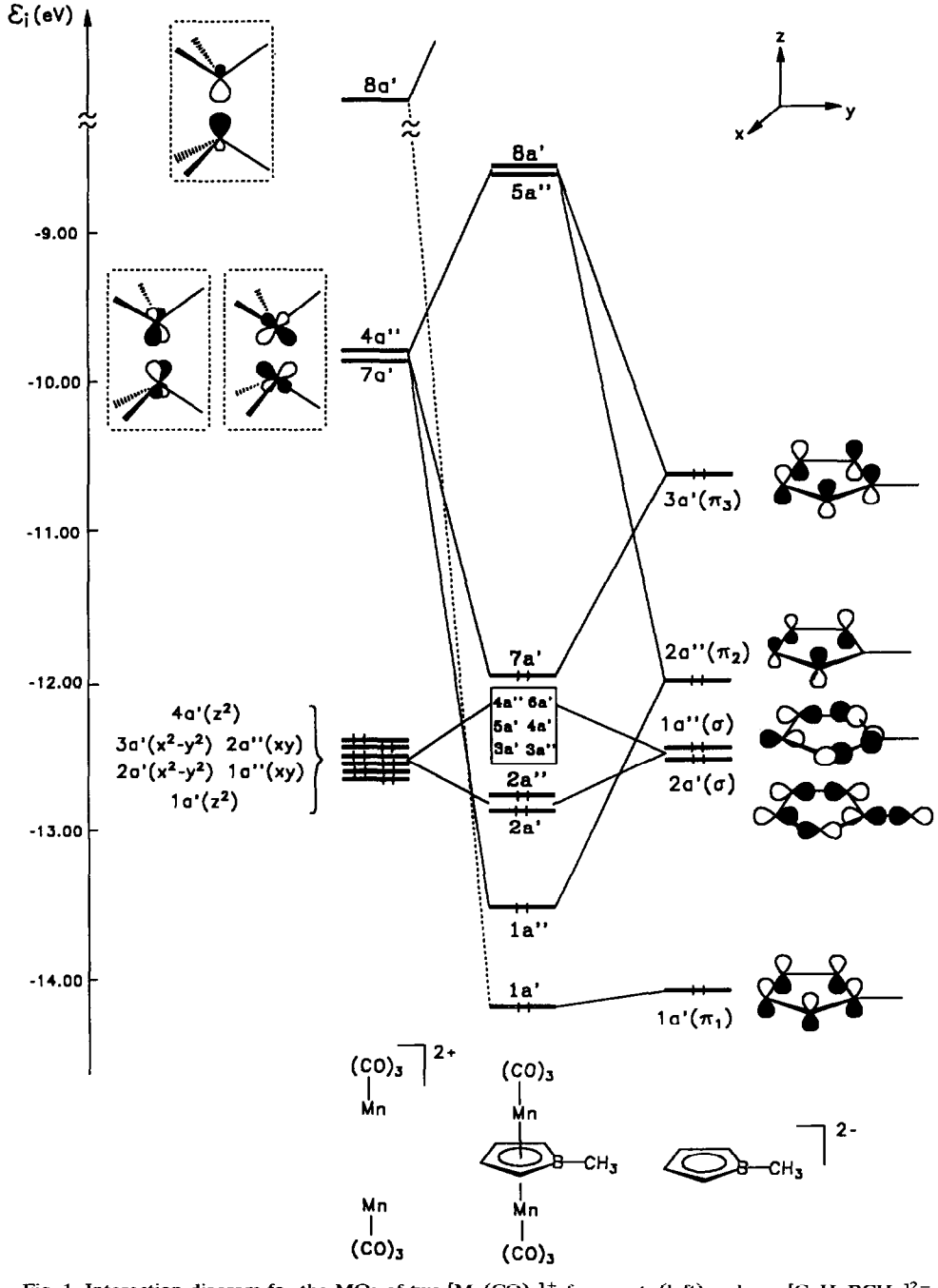

Fig. 1. Interaction diagram for the MOs of two $[Mn(CO)_3]^+$ fragments (left) and one $[C_4H_4BCH_3]^{2-}$ fragment (right) to derive the MOs of **5**.

terms of fragment orbitals with reference to the orbital diagrams of Figs. 1 and 2.

Figure 4 displays the proposed mapping between computed and measured ionization energy. On the low energy side of the PE spectra (7.5–10.5 eV) **5** and **6** display two band systems. In the case of **5** the first band system is composed of two peaks at 8.1 and 8.5 eV. In the case of **6** the maxima of the peaks are located at 7.7 and 8.2 eV with a shoulder at 8.6 eV. The second band system has one peak at 9.8 eV for **5** and two peaks at 9.2 and 9.8 eV for **6**. The ratios of the areas below the envelopes of the two band systems are approximately 6:1 for **5** and 6:1:1 for **6**. The ratios can provide a guide for estimation of the number of ionization events associated with each band system. Beyond 10.5 eV for **5** and 10.1 eV for **6** a broad band is

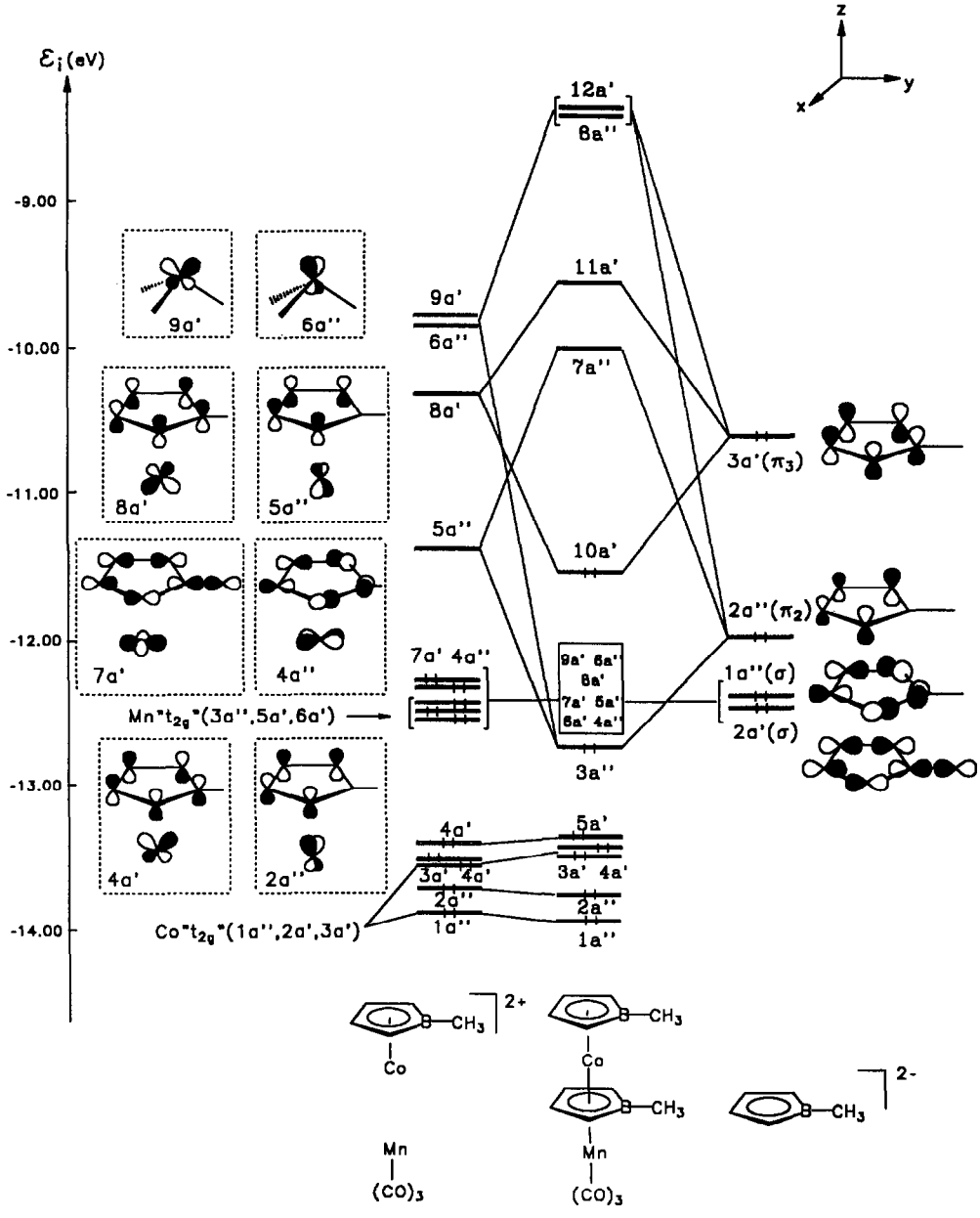

Fig. 2. Interaction diagram for the MOs of one $[Mn(CO)_3]^+$, $[C_4H_4BCH_3)Co]^+$ (left) and one $[C_4H_4BCH_3]^{2-}$ fragment (right) to derive the MOs of **6**.

observed in both PE spectra. Beyond 12.5 eV the PE spectra of **5** and **6** display an intense band, characteristic of the hydrocarbon and carbonyl framework. The computational results listed in Table 1 provide an interpretation of the PE spectra of **5** and **6**. It is seen that with inclusion of relaxation and correlation effects there is a satisfactory correspondence between experimental ionization energies and theoretical results. The key points for understanding the PE spectra of **5** and **6** are the dependence of the Koopmans' defects on (i) the localization of the MO wavefunction at the 3d centre, and (ii) the metal atom. It is well known from previous studies [11,14], that with increasing 3d-participation in the complex MOs enlarged reorganization effects are predicted and also that larger Koopmans' defects are more characteristic of electron-rich metals, for which the 3d-shell becomes extremely contracted [6,11,14]. In the case of **5** the overall effect of relaxation and correlation for ionizations from the "t_{2g}" Mn orbitals leads to an energy decrease of 2.15–3.13 eV with respect to Koopmans' values (Table 1). For ionizations from orbitals with major ligand character the calculated Koopmans' defects have values of < 1.84 eV. Thus, the six ionizations originating in the "t_{2g}" Mn orbitals must be correlated with the first band system of **5** and the third peak must be assigned to an

TABLE 1. Description of the computed vertical ionization potentials I_{vj} at INDO level for **5** and **6**. All energies in eV

MO [a]	$-\epsilon_j$ [b]	Relax [c]	$I_{v,j}^{comp}$ [d]	$I_{v,j}^{exp}$	BAND [e]	Population analysis [f]				
						%Co	%Mn	%L [g]	%CO	fragment and metal orbital assignment
5										
6A′	10.91	2.47	8.44	8.10	1		67	13	20	x^2-y^2
3A″	11.06	2.56	8.50				84	13	3	xy
4A′	11.10	2.57	8.53				68	10	22	z^2
5A′	11.04	2.50	8.54	8.50	2		63	22	15	z^2
3A′	11.71	3.13	8.58				80	10	10	x^2-y^2
4A″	10.86	2.15	8.71				56	25	19	xy
7A′	10.32	0.67	9.65	9.80	3		17	54	29	L: $\pi_3+7a'(yz)$
1A″	12.54	1.84	10.70				48	41	11	L: $\pi_2+4a''(xz)$
2A′	12.21	1.33	10.88	10.60	4		23	72	5	L: σ
2A″	11.94	0.80	11.14				1	94	5	L: σ
1A′	13.17	1.70	11.47				33	50	17	L: π_1+8a'
6										
6A″	10.27	1.48	8.79	7.70	1	1	45	43	11	Mn: xy
4A′	12.25	3.43	8.82			84	–	15	1	Co: z^2
9A′	10.55	1.72	8.83	8.20	2	7	52	26	15	Mn: x^2-y^2
8A′	10.92	2.02	8.90			11	55	30	4	Mn: z^2
3A′	12.67	3.75	8.92	8.60[sh]	3	92	–	7	1	Co: x^2-y^2
5A′	10.25	1.29	8.96			9	36	35	20	L: π_3, π_1
1A″	12.89	3.67	9.22	9.20	4	83	1	6	–	Co: xy
10A′	9.60	0.28	9.32			4	10	79	7	L: π_3+yz
3A″	10.73	0.91	9.82	9.80	5	11	19	65	5	L: π_2+xz
5A″	11.63	1.02	10.61			10	1	87	2	L: σ
4A″	11.66	0.94	10.72			2	11	84	3	L: σ
2A″	12.00	1.05	10.95	10.10	6	20	11	66	3	L: π_2
6A′	11.93	0.89	11.04			5	12	79	4	L: σ
7A′	11.77	0.54	11.23			–	3	96	1	L: σ

[a] The labelling of the valence molecular orbitals refers to Figs. 1 and 2.
[b] Koopmans's ionization potential.
[c] Global influence of relaxation and correlation on the ionization potential.
[d] Computed ionization potential according to eqn. (2).
[e] The numbers refer to the band labelling of Fig. 3.
[f] Mulliken population analysis of the molecular orbitals of the neutral molecule.
[g] $L = C_4H_4BCH_3$.

ionization from the HOMO (7a'). The ionizations arising from the four remaining frontier orbitals of **5** (1a', 2a', 1a'', 2a'') are calculated to be 11.47, 11.14, 10.88 and 10.70 eV, and give rise to the band system starting at 10.5 eV.

We now consider complex **6**, with two different 3d-metals. Analogous to the extended Hückel calculations, the INDO ground state wavefunction of **6**, predicts different localizations and different energies for the 3d-electrons of Co and Mn. The "t_{2g}"-Co orbitals (1a'', 3a', 4a') are strongly localized on the cobalt centre (83–92% Co-3d character) and calculated to be at 12.89, 12.67 and 12.25 eV, respectively. The "t_{2g}" Mn-orbitals (8a', 9a', 6a''), with only 45–55% Mn 3d character, are delocalized, and calculated to be at 10.92, 10.55 and 10.27 eV, respectively. As previously mentioned, large Koopmans' defects can be expected for the "t_{2g}" levels for Co and smaller ones for Mn. The calculated Koopmans' defects are 3.43–3.75 eV and 1.48–2.02 eV for the "t_{2g}"-Co and "t_{2g}"-Mn MOs, respectively. For ionizations originating in ligand orbitals the Koopmans' defects do not exceed 1.05 eV (Table 1). Thus, the six ionizations originating in the "t_{2g}" orbitals of Co and Mn should appear first in the PE spectrum of **6**. We remember that the empirical assignment predicts six ionization events for the first band system of **6**. In this region the INDO calculations predict five ionizations from the metal levels and one from the 5a' MO of **6**. The sixth metal level ionization is calculated to be at 9.22 eV (1a''), exactly at the same value as the maximum of peak 4. The calculated energy separation for the ionizations from the 5a' and 1a'' MO is 0.26 eV, which compares with the experimental value of 0.6 eV.

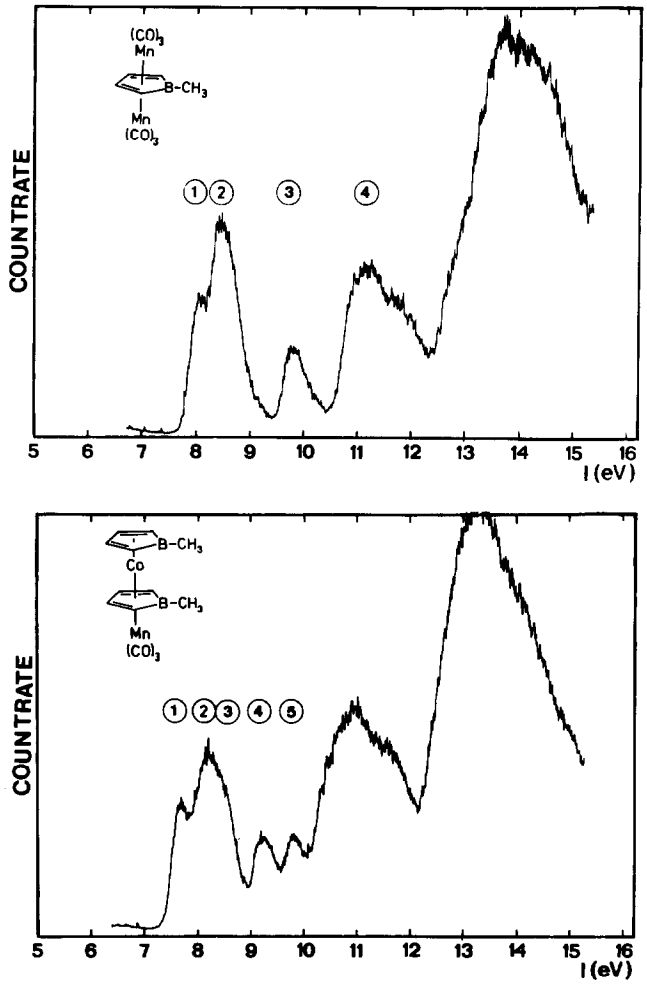

Fig. 3. He(I) photoelectron spectra of **5** and **6**.

It is interesting to note that in the triple-decker complex **4** the lowest ionization from a metal level appears at 9.1 eV and the five remaining metal levels contribute to the first band system with maxima at 7.5 and 8.1 eV [6]. The ionizations from the HOMO and 3a''-MO of **6** are calculated to be at 9.32 and 9.82 eV, compared with the experimental values of 9.2 and 9.8 eV, respectively.

Although experimental assignment predicts one ionization for peak 4, we suggest that for this peak there are two ionizations from the 1a'' and 10a' MOs of **6**. In such cases, where the ionizations from the metal and ligand levels overlap, the "experimental intensity arguments" can be misleading because of the different relaxation effects accompanying these ionizations. The calculated energy separation for peaks 4 and 5 of 0.5 eV agrees well with the experimental value of 0.6 eV. The ionizations arising from the σ-orbitals of both borole ligands and from the π_2-MO of the terminal borole give rise to the band system starting at 10.1 eV (Table 1). The ionizations arising from the π_1-orbitals of the borole ligands are also expected to contribute to this band system. For **6**, the 1a' (π_1) and 2a' (π_1) MOs have not been considered in the particle-hole space of the Green's function method.

In the case of **6** the experimental ionization energy originating from the HOMO (9.2 eV) is lower in energy by 0.6 eV with respect to that for **5** (9.8 eV). The same is true for the ionization from the 3a'' MO. Both findings support the qualitative arguments presented in the preceding section. It is noteworthy that in the triple-decker complex **4** the ionization from the HOMO appears in the broad band system with a maximum at 8.1 eV.

3. Conclusions

The INDO calculations are capable of reproducing the PE pattern of both triple decker compounds when

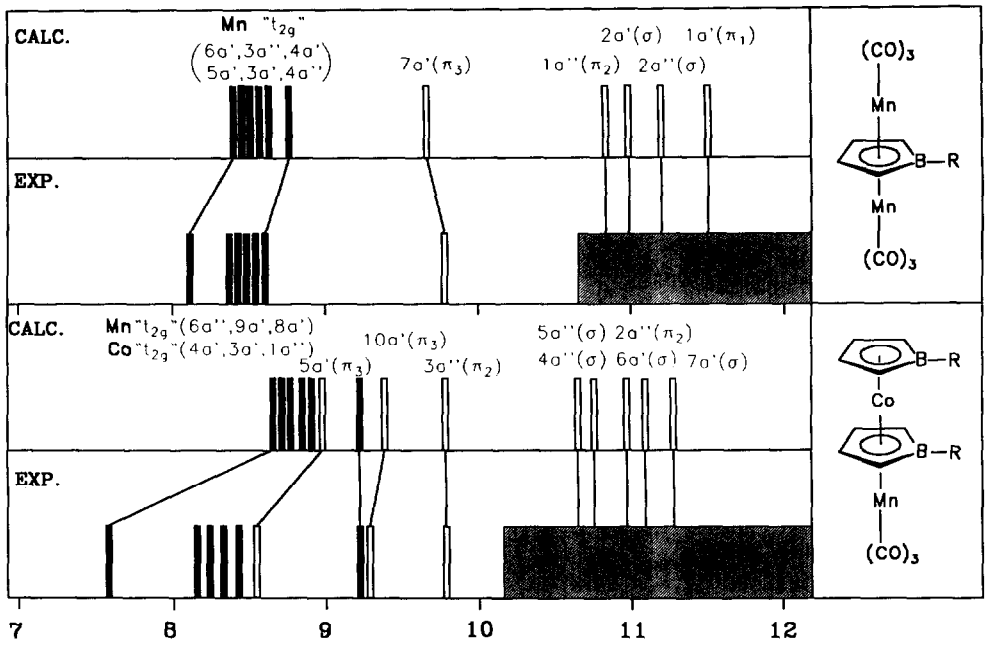

Fig. 4. Correlation between the first PE bands of **5** and **6** with the calculated ionic states.

relaxation effects are taken into account. This in turn increases confidence in the predicted MO sequence shown in Figs. 1 and 2. The main outcome is a stronger stabilization of the HOMO in **5** than in **6**. This stabilization can be traced back to the better overlap between the $Mn(CO)_3$ and the π-system and the better acceptor properties of the $Mn(CO)_3$ unit than in the borole-Co moiety. These effects can be seen by com-

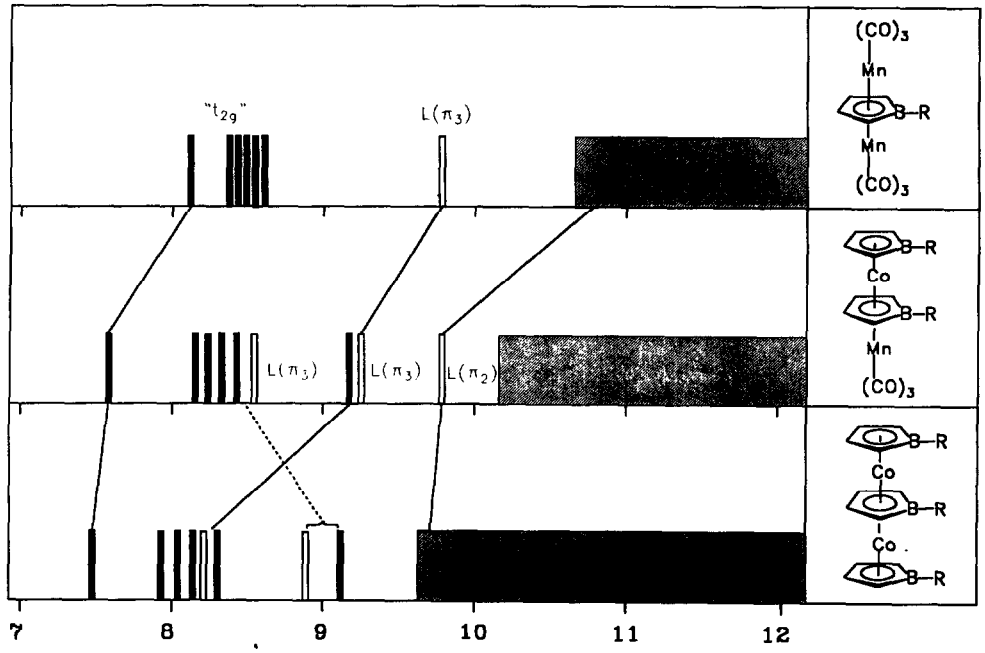

Fig. 5. Correlation between the first PE bands of **5**, **6** and **4**.

paring the first PE bands in **4–6** as shown in Fig. 5. A strong influence of the metal on the ligand MOs is observed.

The MO calculations also provide a delocalized description for the ionic states in the case of the Mn–Mn triple-decker (**5**) and to a lesser extent for **6**. The strongly localized t_{2g} levels of the Co fragment in **6** are subject to greater relaxation effects than for manganese. This is due to the more contracted character of the 3d wave functions of cobalt.

4. Experimental details

Compounds **5** and **6** have been described previously [5]. The He(I) PE spectra of **5** and **6** were recorded with a Perkin-Elmer PS 18 instrument. The recording temperatures were 86° C for **5** and **6**. The calibration was with Ar (15.76 and 15.94 eV) and Xe (12.13 and 13.44 eV). A resolution of 20 meV on the $^2P_{3/2}$ Ar line was obtained.

Acknowledgments

We are grateful to the Deutsche Forschungsgemeinschaft (SFB 247) and the Fonds der Chemischen Industrie for financial support. We thank A. Flatow for recording the PE spectra.

References

1 M.C. Böhm, R. Gleiter, F. Delgado-Pena and D.O. Cowan, *J. Chem. Phys., 79* (1983), 1154; M.C. Böhm, R. Gleiter, F. Delgado-Pena and D.O. Cowan, *Inorg. Chem., 19* (1980) 1081.
2 R. Gleiter, H. Röckel, G. Pflästerer, B. Treptow and D. Kratz, *Tetrahedron Lett., 34* (1993) 8075.
3 A. Fessenbecker, M. Enders, H. Pritzkow, W. Siebert, I. Hyla-Kryspin and R. Gleiter, *Chem. Ber., 124* (1991), 1505; Z. Nagy-Magos, A. Feßenbecker, H. Pritzkow, W. Siebert, I. Hyla-Kryspin and R. Gleiter, *Chem. Ber., 124* (1991) 2685.
4 G.E. Herberich, B. Hessner and R. Saive, *J. Organomet. Chem., 319* (1987) 9.
5 G.E. Herberich, J. Hengesbach, G. Huttner, A. Frank and U. Schubert, *J. Organomet. Chem., 246* (1983) 141; G.E. Herberich, D.P.J. Köffer and K.M. Peters, *Chem. Ber., 124* (1991) 1947.
6 I. Hyla-Kryspin, R. Gleiter, G.E. Herberich and M. Benard, *Organometallics*, in press.
7 T.A. Albright, J.K. Burdett and M.-H. Whangbo, in *Orbital Interaction in Chemistry*, Wiley-Interscience, New York, 1985.
8 R. Hoffmann and W.N. Lipscomb, *J. Chem. Phys., 36* (1962), 2179, 3489; R. Hoffmann and W.N. Lipscomb, *J. Chem. Phys., 37* (1962) 2872; R. Hoffmann, *J. Chem. Phys., 39* (1963) 1397.
9 R.H. Summerville and R. Hoffmann, *J. Am. Chem. Soc., 98* (1976) 7240.
10 M.C. Böhm and R. Gleiter, *Theoret. Chim. Acta, 59* (1981) 127, 153.
11 M. Doran, I.H. Hillier, E.A. Seddon, K.R. Seddon, V.H. Thomas and M.F. Guest, *Chem. Phys. Lett., 63* (1979) 612; I.H. Hillier, *Pure Appl. Chem., 51* (1979) 2183.
12 M.C. Böhm, R. Gleiter and C.D. Batich, *Helv. Chim. Acta, 63* (1980) 990; M.C. Böhm and R. Gleiter, *J. Comput. Chem., 3* (1982) 140; M.C. Böhm, *Theoret. Chim. Acta, 61* (1982) 539; C. Cauletti, J.C. Green, M.R. Kelly, P. Powell, J. van Tilborg, J. Robbins and J. Smart, *J. Electron. Spectrosc. Relat. Phenom., 19* (1980) 327.
13 A. Veillard and J. Demuynck in H.F. Schaefer (ed.), *Modern Theoretical Chemistry Vol. 4*, Plenum Press, New York, 1977; H. Van Dam and A. Oskam UV Photoelectron Spectroscopy of Transition Metal Complexes, in G.A. Melson and B.N. Figgis (eds.), *Transition Metal Chemistry, Vol. 9*, Marcel Dekker, New York, 1985, pp. 125–308.
14 F. Ecker and G. Hohlneicher, *Theoret. Chim. Acta, 25* (1972) 289; P.O. Nerbrant. *Int. J. Quantum Chem., 9* (1975) 901; L.S. Cederbaum, *Theoret. Chim. Acta, 31* (1973) 239; L.S. Cederbaum, *J. Phys. B., 8* (1975) 290; L.S. Cederbaum and W. Domcke, *Adv. Chem. Phys., 36* (1977) 205; W.v. Niessen, L.S. Cederbaum, W. Domcke, J. Schirmer, in J. Bargon (ed.), *Computational Methods in Chemistry*, Plenum Press, New York, 1980.
15 M.C. Böhm, R. Gleiter, G.E. Herberich and B. Hessner, *J. Phys. Chem., 89* (1985) 2129 and references therein; M.C. Böhm and R. Gleiter, *Chem. Phys. Lett., 123* (1986) 87; M.C. Böhm and R. Gleiter, *Theoret. Chim. Acta, 57* (1980) 315.
16 F. Dyson, *J. Phys. Rev., 75* (1949) 486.
17 R. Gleiter, I. Hyla-Kryspin, M.L. Ziegler, G. Sergeson, J.C. Green, L. Stahl and R.D. Ernst, *Organometallics, 8* (1989) 298; R. Gleiter, I. Hyla-Kryspin, P. Binger and M. Regitz, *Organometallics, 11* (1992) 177.
18 D.A. Taylor, I.H. Hillier, M. Vincent, M.F. Guest, A.A. MacDowell, W.v. Niessen and D.S. Urch, *Chem. Phys. Lett., 121* (1985) 482.
19 J.W. Lauher, M. Elian, R.H. Summerville and R. Hoffmann, *J. Am. Chem. Soc., 98* (1976) 3219.